INDIAN INSTITUTE OF TECHNOLOGY BOMBAY

Probing Beyond Standard Model neutrino interactions with IceCube DeepCore

---

Author:

Samyak Jain[1, 2]

Supervisors:

Sebastian Böser[1]

Vikram Rentala[2]

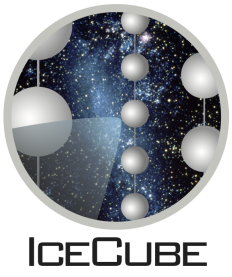

[1]Johannes Gutenberg University of Mainz

[2]Indian Institute of Technology Bombay

Wednesday, 10th April, 2024

Declaration

I declare that this written submission represents my ideas in my own words and where others ideas or words have been included, I have adequately cited and referenced the original sources. I also declare that I have adhered to all principles of academic honesty and integrity and have not misrepresented, fabricated, or falsified any idea/data/fact/source in my submission. I understand that any violation of the above will be cause for disciplinary action by the Institute and can also evoke penal action from the sources which have thus not been properly cited or from whom proper permission has not been taken when needed.

Samyak Jain
200260046

Friday 16th August, 2024

Abstract

Simultaneous sensitivities of IceCube to Non-Standard neutrino interactions (NSI) are presented. The nature of this work is similar to [1], but uses 9.28 years of IceCube data as opposed to 2.5 years. The higher sensitivities reveal nuances in the NSI + detector/flux parameter space, and the minimization procedure used in [1] is found to be inadequate. A minimization procedure to recover NSI hypotheses reasonably well is outlined, and the corresponding sensitivities to the no-NSI hypothesis are presented.

Acknowledgements

I wish to record a deep sense of gratitude for Sebastian Böser for encouraging my passion for fundamental physics, as well as providing numerous opportunities to forge valuable connections in the high energy physics community. I am also grateful to the Mainz neutrino group for providing an incredibly welcoming environment. I would like to thank Veronika Palusova, Jan Weldert, Finn Mayhew, and Shiqi Yu for their help in conducting this analysis. I would also like to thank Kaustav Dutta and John Rack-Helleis for fruitful discussions. Lastly, I wish to thank Tyce DeYoung and the Michigan State University for providing access to their cluster for this analysis.

Table of Contents

List of Figures

List of Tables

Chapter 1

Introduction

The Standard Model (SM) of particle physics represents the culmination of decades of research, and is the best description of particle physics we have to date. However, several inconsistencies of SM with experimental results are well known, and Beyond Standard Model (BSM) physics presents various exciting new avenues to pursue. One of the most notable such avenues is the inability of the SM to explain neutrino masses and neutrino oscillations.

The IceCube Neutrino Observatory at the South Pole, initially constructed to identify astrophysical neutrino sources, has also turned into a wonderful particle physics experiment. The vast range of oscillation baselines to available to IceCube, from ~ 0 upto the Earth diameter, make it uniquely sensitive to neutrino oscillations. Further, since IceCube does not utilize a fixed neutrino source, it is not particularly flavor bound.

Most importantly for this analysis, the large oscillation baselines available to IceCube pass through different lengths inside the Earth, which allows for oscillation probabilities to be significantly tuned by matter effects. This makes IceCube uniquely sensitive to neutrino NSI; unlike other neutrino experiments, IceCube is sensitive to multiple NSI

parameters.

Constraints on neutrino NSI using 2.5 years of IceCube data were previously placed in [1]. We wish to improve upon these results using 9.28 years of IceCube data. However, we find that the better reconstruction algorithms and our higher sensitivities reveal nuances in the NSI + experimental parameter space that make minimization of a metric in the parameter space extremely difficult, in particular, the simplistic minimization procedure used in [1] is found to be inadequate.

This analysis thus significantly draws on the work of Elisa Lohfink [2], who modeled NSI sensitivities using the same dataset as used for this analysis. However, due to computational constraints, only one NSI parameter (out of 8) was constrained at a time in [2].

This work is thus a confluence of the two analyses, we provide simultaneous NSI sensitivities as in [1], using a reparameterization of NSI effects (the Generalized Matter Potential), with a minimization procedure motivated from the findings in [2].

First, the formalism of neutrino oscillations, motivated by non-zero neutrino masses, along with the parameterization of matter and NSI effects, is discussed in Section 2. A reparameterization of NSI effects, the Generalized Matter Potential is discussed in Section 3. A short discussion of neutrino detection in IceCube, along with the observables of this analysis, is is given in Section 4. Finally, the details of the analysis, along with the minimization procedure to recover NSI hypotheses, and the final NSI sensitivities, are presented in Section 5.

Chapter 2

Neutrinos Beyond the Standard Model

The evidence of neutrino masses and neutrino oscillations are one of the most important indicators for BSM physics. Evidence of neutrino oscillations were first detected in the 1990's by the Homestake experiment's observation of the solar neutrino deficit: the solar neutrino flux measured was significantly lower than the predicted values. Only electron neutrinos are expected to be generated in the sun, which is what the experiment was sensitive to. This was resolved by positing that neutrino flavor states could oscillate between each other as the neutrino propagate through space.

As shown below, neutrino oscillations indicate massive and non-degenerate neutrino mass eigenstates. In this section, we first establish the formalism for neutrino oscillations, and then account for the effect of standard (within the SM) matter interactions on the oscillations. Finally, we generalize the effect of interactions to include Non-Standard Interactions (BSM).

2.1 Neutrino oscillations in vacuum

A simple picture of neutrino oscillations is as follows: let us consider the neutrino flavor fields ν_α to be linear combinations of non-identical mass fields ν_i. Considering a neutrino of momentum p propagating in space, the mass eigenstates will have separate energies given by

$$E_i = p + \frac{m_i^2}{2E}, \quad E \approx p \tag{2.1}$$

where we assume the neutrino to be ultra-relativistic, and E is the neutrino energy. Thus, in the time evolution of an initial flavor eigenstate $|\nu_\alpha\rangle$, the phases of the various mass eigenstates will oscillate with different frequencies, leading to oscillating phase differences, which in turn leads to an oscillating probability of observing the neutrino in some other flavor state $|\nu_\beta\rangle$.

The matrix connecting the two basis of the neutrino *fields* is the Pontecorvo Maki Nakagawa Sakata mixing matrix (PMNS-matrix) U:

$$\nu_\alpha = U_{\alpha i}\nu_i \tag{2.2}$$

$$U = \begin{pmatrix} 1 & 0 & 0 \\ 0 & c_{23} & s_{23} \\ 0 & s_{23} & c_{23} \end{pmatrix} \begin{pmatrix} c_{13} & 0 & s_{13}e^{-i\delta_{\text{CP}}} \\ 0 & 1 & 0 \\ -s_{13}e^{i\delta_{\text{CP}}} & 0 & c_{13} \end{pmatrix} \begin{pmatrix} c_{12} & s_{12} & 0 \\ -s_{12} & c_{12} & 0 \\ 0 & 0 & 1 \end{pmatrix} \tag{2.3}$$

where

$$c_{ij} = \cos\theta_{ij}, s_{ij} = \sin\theta_{ij} \tag{2.4}$$

and θ_{ij} are the so called mixing angles. Non-zero values of δ_{CP} imply CP (charge and parity) violating effects.

The time evolution of the flavor eigenstates is then given by

$$|\nu_\alpha(t)\rangle = U^*_{\alpha i} |\nu_i(t)\rangle \tag{2.5}$$

where

$$|\nu_i(t)\rangle = e^{-iE_i t} |\nu_i(0)\rangle \tag{2.6}$$

Thus, the probability of the in initial flavor state $|\nu_\alpha\rangle$ to interact as the flavor states $|\nu_\beta\rangle$ is

$$\begin{aligned} P_{\alpha\beta} &= |\langle \nu_\beta | \nu_\alpha(t) \rangle|^2 \\ &= \sum_{ij} U^*_{\alpha i} U_{\beta i} U_{\alpha j} U^*_{\beta j} \exp\left(-i \frac{\Delta m^2_{ij} t}{2E}\right) \end{aligned} \tag{2.7}$$

where

$$\Delta m^2_{ij} = m^2_i - m^2_j \tag{2.8}$$

It is conventional to use the neutrino propagation distance L (also known as the oscillation baseline)

$$L \approx ct \tag{2.9}$$

instead of the propagation time t to describe neutrino oscillations. Upon simplifying,

one obtains

$$P_{\alpha\beta}(L,E) = \delta_{\alpha\beta} - 4\sum_{i>j} Re(U^*_{\alpha i}U_{\beta i}U_{\alpha j}U^*_{\beta j})\sin^2\left(\frac{\Delta m^2_{ij}L}{4E}\right) + 2\sum_{i>j} Im(U^*_{\alpha i}U_{\beta i}U_{\alpha j}U^*_{\beta j})\sin\left(\frac{\Delta m^2_{ij}L}{2E}\right) \tag{2.10}$$

We can also construct the Hamiltonian H_{vac} governing the time evolution of the flavor states. We have

$$\begin{aligned} i\frac{d}{dt}|\nu_\alpha\rangle &= U^*_{\alpha i}\frac{d}{dt}\left(i|\nu_i\rangle\right) \\ &= U^*_{\alpha i}\left(E_i|\nu_i\rangle\right) \\ &= U^*_{\alpha i}E_i U^\dagger_{i\beta}|\nu_\beta\rangle \end{aligned} \tag{2.11}$$

Writing this in matrix form, we have

$$i\frac{d}{dt}|\nu_\alpha\rangle = \left(U^*\text{diag}(E_1,E_2,E_3)U^\dagger\right)_{\alpha\beta}|\nu_\beta\rangle \tag{2.12}$$

Now, as seen in the calculation of probabilities, only the differences in the energies E_i contribute to the phase differences. Thus, we can ignore the p term in Eq.(2.1) and substitute in Eq.(2.12) to obtain

$$i\frac{d}{dt}|\nu_\alpha\rangle = \frac{1}{2E}\left(U^*\text{diag}(m^2_1,m^2_2,m^2_3)U^\dagger\right)_{\alpha\beta}|\nu_\beta\rangle \tag{2.13}$$

Thus, we have the vacuum Hamiltonian H_{vac} as

$$H_{\text{vac}} = \frac{1}{2E}U^*\text{diag}(m^2_1,m^2_2,m^2_3)U^\dagger \tag{2.14}$$

When considering matter effects, we shall incorporate them as a perturbation to the

vacuum Hamiltonian.

2.2 Neutrino masses

As evident in Eq.(2.10), the probabilities depend on the mass-squared differences of the mass eigenstates. Obviously, only two independent squared mass differences are needed, these are chosen as Δm^2_{21} and Δm^2_{31}. By convention, Δm^2_{21} is chosen to be positive. This choice allows for either $\Delta m^2_{31} > 0$ (the Normal Ordering of neutrino masses, or NO), or $\Delta m^2_{31} < 0$ (Inverted Ordering, or IO). The two orderings are pictorially shown in Fig.2.1.

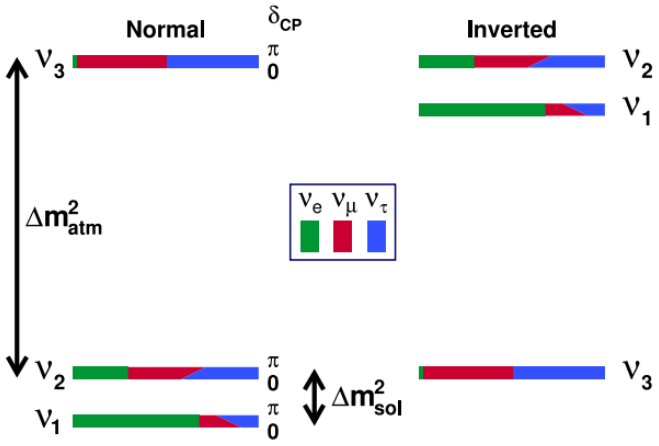

Figure 2.1: Taken from [2]. "Schematic overview of the mass-squared differences in normal (left) and inverted (right) ordering, adapted from [24]. Heavier states are further at the top of the drawing. For normal ordering, the (larger) atmospheric mass splitting and (smaller) solar mass splitting are indicated. The neutrino flavor state content of the individual mass eigenstates is indicated in color. The dependence on Î´CP is represented for values of 0 and π at the lower and upper border, respectively, of the individual bars, yielding tilted edges. "

2.3 Standard Matter effects

When transversing matter, neutrinos can undergo forward scattering with the matter constituents. This creates an effective potential seen by the propagating neutrino, which can be included as a perturbation to the vacuum Hamiltonian.

When transversing matter consisting of e^-, p^+, n_0, neutrinos can undergo forward scattering with each of them. In particular, all the flavors can undergo forward scattering with e^-, p^+, n_0 through the neutral current (NC). However, electron neutrinos can undergo forward scattering with e^- via the charged current (CC) as well. The diagrams describing these processes are given in Fig.2.2.

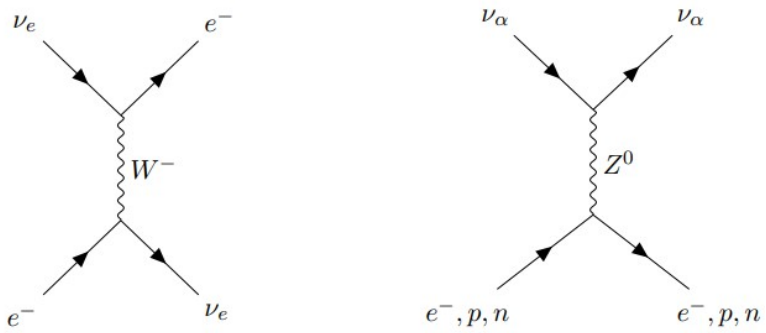

Figure 2.2: Figure taken from [2]. "Forward scattering of neutrinos on regular matter as included in the SM. While NC scattering (right diagram) is possible for all neutrino flavors, electron neutrinos can also undergo CC scattering (left diagram) on surrounding electrons. "

Thus the effective potential seen by the propagating neutrino can be written as

$$V(x) = \text{diag}\left(V_e^{\text{CC}}(x) + V_e^{NC}(x), V_\mu^{NC}(x), V_\tau^{NC}(x)\right) \tag{2.15}$$

Since all the NC interactions occur with all of e^-, p^+, n_0, the NC potentials are identical. Since inter-flavor oscillations will be affected by only the differences of the corresponding potentials, we can subtract the NC potential from all the diagonal elements and

obtain

$$H_{\text{mat}}(x) = V(x) = \text{diag}(V_{\text{CC}}(x), 0, 0) = \sqrt{2}G_F N_e \text{diag}(1,0,0) \tag{2.16}$$

where N_e is the electron density at position x (one would intuitively expect the CC potential to be proportional to the spatial electron density), and G_F is Fermi's coupling constant.

Thus for a neutrino propagating through matter, the Hamiltonian governing the evolution of the flavor states is given by

$$H_\nu = H_{vac} + H_{mat}(x) \tag{2.17}$$

and for antineutrinos, the corresponding Hamiltonian is [2]

$$H_\nu = [H_{vac} - H_{mat}(x)]^* \tag{2.18}$$

Thus, one may now calculate oscillations probabilities as before using the total Hamiltonian.

2.4 Non Standard Interactions

Non-Standard Interactions (NSI) refer to any matter interactions not accounted for in the SM. One would then expect the SM to be a low-energy limit of some BSM theory, whose effects are suppressed at SM energies.

Now, one may come up with a myriad of new theories that use new particles or new interaction channels that give rise to NSI. The results of such an approach would be extremely dependent on the theory's parameters. Fortunately, we need not constrain

ourselves to a specific model, and instead work with a largely general parameterization of NSI effects.

We can assume that the most dominant NSI effects arise from coherent forward scattering of neutrinos with fermions present in the matter it is propagating through. NSI can again go through the charged or neutral currents. One can formulate the four-fermion Lagrangians describing forward scattering NSI as [3]

$$\mathcal{L}_{\text{NC-NSI}} = -2\sqrt{2}G_F\varepsilon^{fC}_{\alpha\beta}\left(\bar{\nu}_\alpha\gamma^\mu P_L\nu_\beta\right)\left(\bar{f}\gamma_\mu P_C f\right) \tag{2.19}$$

$$\mathcal{L}_{\text{CC-NSI}} = -2\sqrt{2}G_F\varepsilon^{ff'X}_{\alpha\beta}\left(\bar{\nu}_\alpha\gamma_\mu P_L l_\beta\right)\left(\bar{f}'\gamma^\mu P_C f\right) \tag{2.20}$$

where f, f' indicate the fermions involved, and there is a summation over f, f' with $f \neq f'$, as well as the chiralities X, C. Here, $\varepsilon_{\alpha\beta}$ are scalar coupling strengths that indicate how strong each interaction is. It has been shown that CC interactions affect mostly the production and detection of neutrinos, and thus have a stronger impact on experiments with neutrino sources whose flux are well known. Atmospheric neutrinos, which are the focus of this study are more sensitive to effects during neutrino propagation. In particular, NSI forward scattering through NC interaction would have the most significant effect on our results.

Thus, our parameters of interest are $\varepsilon^{fC}_{\alpha\beta}$. For matter propagation, it can be shown that only the vector part of the NSI couplings is relevant, which translates to [4]

$$\varepsilon^{f}_{\alpha\beta} = \varepsilon^{fL}_{\alpha\beta} + \varepsilon^{fR}_{\alpha\beta} \tag{2.21}$$

Then, akin to Eq.(2.16), the effective NSI potential as seen by a neutrino propagating through matter consisting of various fermions would be

$$V_{\text{NSI},\alpha\beta}(x) = \sqrt{2}G_F N_e(x)\varepsilon_{\alpha\beta}(x) \tag{2.22}$$

where we define

$$\varepsilon_{\alpha\beta}(x) = \varepsilon^f_{\alpha\beta}\frac{N_f(x)}{N_e(x)} \tag{2.23}$$

In Earth, the fermions of interest are e^-, u, d. The densities of u and d are obtained via the proton and neutron densities in the Earth. Neutrality of Earth implies $N_e = N_p$, and the neutron-electron density ratio in the Earth is nearly uniform

$$Y_n^{\oplus} = \langle N_n(x)/N_e(x)\rangle \approx 1.051 \tag{2.24}$$

From Eq.(2.23), one then obtains

$$\varepsilon_{\alpha\beta}(x) = \varepsilon^e_{\alpha\beta} + \varepsilon^p_{\alpha\beta} + Y_n^{\oplus}\varepsilon^n_{\alpha\beta} \tag{2.25}$$

where $\varepsilon^p_{\alpha\beta}, \varepsilon^n_{\alpha\beta}$ are the appropriately scaled combinations of $\varepsilon^u_{\alpha\beta}$ and $\varepsilon^d_{\alpha\beta}$.

We can now simply add the NSI potential as parameterized in Eq.(2.22) to the matter potential we computed in Eq.(2.16) to obtain the new H_{mat}. Imposing Hermiticity on H_{mat}, we obtain

$$H_{\text{mat}}(x) = \sqrt{2} G_F N_e(x) \begin{pmatrix} 1+\varepsilon_{ee} & \varepsilon_{e\mu} & \varepsilon_{e\tau} \\ \varepsilon^*_{e\mu} & \varepsilon_{\mu\mu} & \varepsilon_{\mu\tau} \\ \varepsilon^*_{e\tau} & \varepsilon^*_{\mu\tau} & \varepsilon_{\tau\tau} \end{pmatrix} \tag{2.26}$$

where $\varepsilon_{\alpha\beta}$, as defined in Eq.(2.25), are our parameters of interest. Note that the off-diagonal element of H_{mat} are complex and describe interactions where the ingoing and outgoing flavors are different. On the other hand, the diagonal terms are real, and describe interactions in which the in-going and outgoing flavors are identical. The diagonal terms allow for the breaking of flavor-universality, and are often referred to as the flavor diagonal (FD) parameters.

It can be shown that oscillation experiments are not sensitive to all the FD parameters, but only for a potential flavor non-universality [5]. In other words, one may subtract any multiple of the identity matrix from the oscillation Hamiltonian. By convention, one can subtract $\varepsilon_{\mu\mu}\mathbb{I}$ to turn the $\mu\mu$ component to 0. We then have

$$H_{\text{mat}} = \sqrt{2} G_F N_e(x) \begin{pmatrix} 1+\varepsilon_{ee}-\varepsilon_{\mu\mu} & \varepsilon_{e\mu} & \varepsilon_{e\tau} \\ \varepsilon^*_{e\mu} & 0 & \varepsilon_{\mu\tau} \\ \varepsilon^*_{e\tau} & \varepsilon^*_{\mu\tau} & \varepsilon_{\tau\tau}-\varepsilon_{\mu\mu} \end{pmatrix} \tag{2.27}$$

Thus, we have 2 real parameters ($\varepsilon_{ee}-\varepsilon_{\mu\mu}, \quad \varepsilon_{\tau\tau}-\varepsilon_{\mu\mu}$) and 3 complex parameters (the cross terms). Each complex parameter has a magnitude and a phase, amounting to a total of 8 real parameters.

Chapter 3

Reparameterizing NSI: the Generalized Matter Potential

As mentioned in the Section 1, IceCube is uniquely sensitive to multiple NSI parameters, in contrast to other experiments which are usually sensitive to only one NSI parameter. Consequently, IceCube is uniquely capable of constraining several NSI parameters simultaneously.

However, minimization with all the NSI parameters, along with detector systematics and other oscillation parameters, is computationally infeasible. As shown in [2], inject-recovery (recovering a NSI hypothesis via minimization in the parameter space) is very challenging with even one NSI parameter. We would thus like to simplify our NSI parameterization, while still preserving the generality of the approach.

As shown in [6], one solution is to adopt the Generalized Matter Potential, which is a reparameterization of the matter Hamiltonian in Eq.(2.27). The fundamental inspiration behind this parameterization is to decompose the matter Hamiltonian into rotation matrices which govern oscillations from one flavor to another, just as is done for PMNS

matrix in Eq.(2.3).

It has been shown [7] that there is a strong cancellation of neutrino oscillations when two eigenvalues of the matter Hamiltonian are degenerate. Thus, under this assumption, one can place the weakest possible constraints on the NSI parameters despite the underlying assumption.

Under this regime, H_{mat} can be written in terms of a scalar strength ε, two rotation angle ϕ_{12}, ϕ_{13}, and two CP violating phases α_1, α_2. The decomposition is [6]

$$H_{\text{mat}} = Q_{\text{rel}} U_{\text{mat}} D_{\text{mat}} U_{\text{mat}}^{\dagger} Q_{\text{rel}}^{\dagger} \tag{3.1}$$

where

$$\begin{aligned} Q_{\text{rel}} &= \text{diag}\left(e^{i\alpha_1}, e^{i\alpha_2}, e^{-i(\alpha_1+\alpha_2)}\right) \\ U_{\text{mat}} &= R_{12}(\phi_1 2) R_{13}(\phi_{13}) \\ D_{\text{mat}} &= \sqrt{2} G_F N_e(x) \text{diag}(\varepsilon, 0, 0) \end{aligned} \tag{3.2}$$

This parameterization of NSI effects is known as the Generalized Matter Potential (referred to as the GMP in the rest of this work). One can show that the two NSI parame-

terizations are related by [6]

$$\begin{aligned}
\varepsilon_{ee} - \varepsilon_{\mu\mu} &= \varepsilon \left(\cos^2 \phi_{12} - \sin^2 \phi_{12}\right) \cos^2 \phi_{13} - 1 \\
\varepsilon_{\tau\tau} - \varepsilon_{\mu\mu} &= \varepsilon \left(\sin^2 \phi_{13} - \sin^2 \phi_{12} \cos^2 \phi_{13}\right) \\
\varepsilon_{e\mu} &= -\varepsilon \cos \phi_{12} \sin \phi_{12} \cos^2 \phi_{13} e^{i(\alpha_1 - \alpha_2)} \\
\varepsilon_{e\tau} &= -\varepsilon \cos \phi_{12} \cos \phi_{13} \sin \phi_{13} e^{i(2\alpha_1 + \alpha_2)} \\
\varepsilon_{\mu\tau} &= \varepsilon \sin \phi_{12} \sin \phi_{12} \cos^2 \phi_{13} e^{i(\alpha_1 + 2\alpha_2)}
\end{aligned} \tag{3.3}$$

IceCube has little sensitivity to α_1, α_2, thus they can be set to 0. We are finally left with 3 free parameters, $\varepsilon, \phi_{12}, \phi_{13}$. Any constraints we obtain on these can be translated to constraints on $\varepsilon_{\alpha\beta}$ using Eq.(3.3).

Due to various symmetries in the GMP parameter space, one need not consider the most general $(0, 2\pi)$ range of the rotation angles. As shown in [6], for the case of real NSI $(\alpha_1 = \alpha_2 = 0)$, one may reduce the range of ϕ_{12}, ϕ_{13} to $\left(-\frac{\pi}{2}, \frac{\pi}{2}\right)$.

No such bounds on ε exist. In particular, one can show [6] that the oscillation probabilities only depend on the total sign of $\Delta m^2_{31}.\varepsilon$, and not their individual signs. This allows this analysis to simultaneously investigate both mass orderings (unlike [2], which considers only the NO), by keeping Δm^2_{31} positive, and allowing for ε to be both positive and negative. Since we expect NSI effects to be weak, one would expect the true value of ε to be close to that of the case of Standard Oscillations, that is $\varepsilon = \pm 1$ (-1 corresponds to Standard Oscillations with the IO). For this analysis, we generously choose the range of ε as (-10, 10). For future work however, one may consider reducing this range, as ε is one of the most influential parameters of this analysis, and large ranges can lead to exceedingly high computation times.

Chapter 4

Neutrinos in IceCube

Atmospheric neutrinos detected in IceCube arrive from various incoming directions. Consequently, depending on the angle θ the incoming direction makes with the Earth axis, neutrinos observe a wide range of oscillation baselines, from a few kilometers up to the Earth diameter, as well as a wide range of the strength of matter effects due to the increasing matter density closer to the Earth's core. This is schematically shown in Fig.(4.1). By convention, $\cos(\theta) = -1$ for neutrinos passing through the entire earth before reaching IceCube (upgoing), and $\cos(\theta) = 0$ for neutrinos produced at the South Pole (downgoing).

IceCube utilizes a cubic kilometer of Antarctic ice as a massive Cherenkov tank for neutrino detection. Neutrinos can interact with matter through a variety of channels (see Section 2.2 of [2] for more details). These interactions can produce various charged secondaries, and for high enough neutrino energies, these secondaries may move faster than the phase velocity of light in the ice. These charged particles then emit Cherenkov radiation, which is then detected by IceCube detectors. The optical properties of the ice allow for the Cherenkov radiation emitted in the neutrino interaction (event) to be detected at large distances due to a low absorption coefficient of the ice.

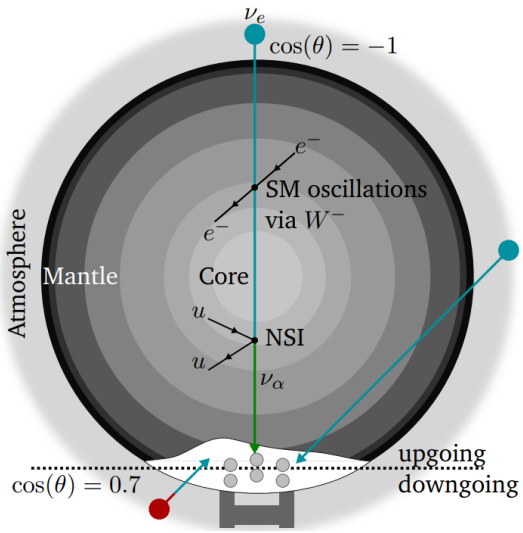

Figure 4.1: The wide range of oscillation baselines that IceCube enjoys is shown. Along with the geometrically increasing propagation lengths in the Earth, the layered structure of the Earth makes different incoming neutrino directions experience different strengths of matter effects. Stanadard matter effects and NSI effects are shown schematically as well. Figure taken from [2].
"Schematic of SM and NSI based matter oscillations effects on atmospheric neutrinos. After being produced inside the atmosphere, neutrinos traverse Earth matter at baselines that depend on their zenith angle θ before potentially being detected inside IceCube. The baselines within layers of different density impact the oscillations behavior through the local electron and nucleon density. Within the SM, matter effects on oscillations are induced through CC scattering of electron neutrinos on electrons (see section 3.2.3). The NSI considered in this work comprise NC forward scattering of all neutrino flavors on first generation charged fermions."

Each event can be parameterized by the neutrino energy, the incoming direction θ of the neutrino (relative to the Earth's axis), and the neutrino flavor. Interactions of different neutrino flavours produce various photon patterns in the ice. NC interactions of all flavors produce hadronic cascades, while CC interactions of different flavors may produce different signatures. CC interactions produce leptons of the same flavour as the incoming neutrino, and the decay of this lepton leaves distinct signatures in the ice. As discussed in Section 4.4 of [2], for the relevant GeV energy scales, and given the resolution of IceCube DeepCore, electron and tau neutrino CC interactions are seen as

cascades, while muon neutrino CC interactions leave a track-like signature (most of the energy of the muon decay is deposited along an elongated path in the ice). This makes IceCube especially sensitive to muon neutrino CC interactions. Different types of interaction signatures are shown in Fig.4.2

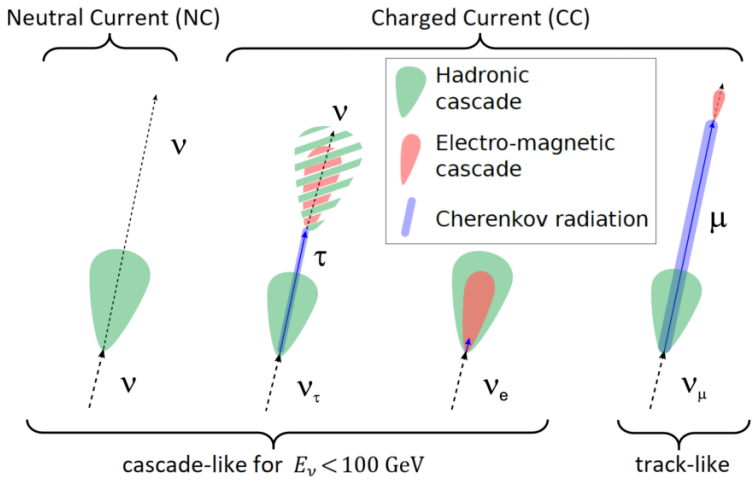

Figure 4.2: Neutrino signatures in IceCube for different flavors and different interaction channels. Figure taken from [2].
"Photon signatures of neutrino events, with the interaction type indicated above and the topology as seen by IceCube indicated below. Modified from [77]."

Thus, the observable of this analysis is the number of neutrino interactions detected (events) binned in neutrino energy, incoming direction θ, and PID (particle identification), which classifies an event as cascade-like, track-like, or mixed (has signatures of both profiles). Different choices of parameters create different binned counts, using which we shall place our constraints.

Evidently, there are many more parameters apart from those discussed here which are relevant to simulating events in IceCube. These include detector systematics, ice properties, atmospheric neutrino and lepton fluxes etc, with various working groups modelling various parameters. These are all simulated in the PINGU Simulation and Analysis

(PISA) framework, a collaborative effort of all IceCube oscillation groups, where each group contributes their implementation of their parameters of interest (so called 'physics parameters'). Thus, the theory and implementation of the remaining 'nuisance parameters' of this analysis are not discussed here; a brief discussion on the same can be found in [2]. The nominal values (current best estimate) and the uncertainties of the nuisance parameters are taken as currently available in PISA.

As discussed earlier, the no-NSI case (referred to as Standard Oscillations) is found at $\varepsilon = 1, \phi_{12} = \phi_{13} = 0$. In Fig.4.3, oscillation probabilities $P_{\alpha\to\mu}$ are plotted in the $\cos(\theta) - E$ space for the Standard Oscillations case, with PMNS matrix parameters and the other nuisance parameters set to their nominal values. The nominal values and ranges of the PMNS matrix and nuisance parameters considered in this analysis can be found in Table 5.1. The sharp change in oscillation probabilities seen at $\cos\theta \approx -0.8$ is due to the sudden change in the matter density at the core-mantle interface.

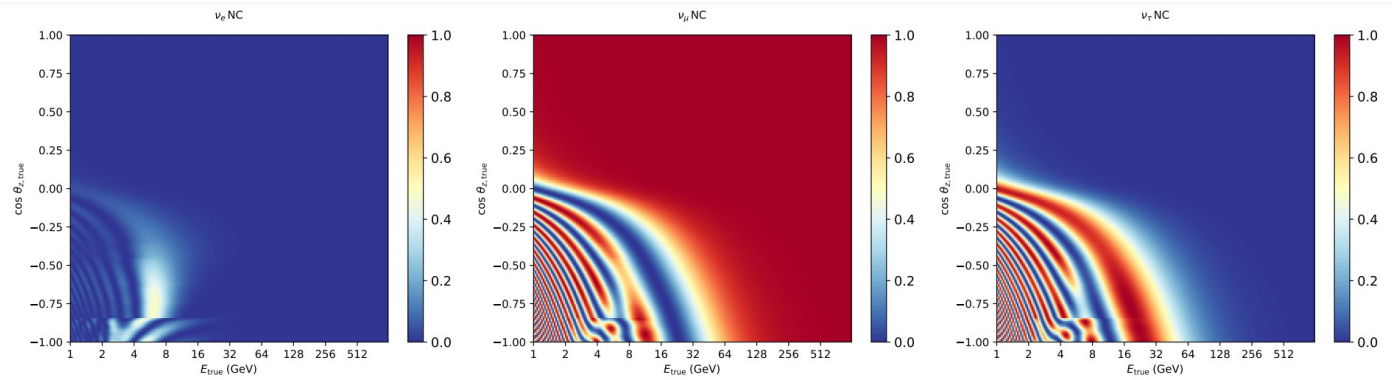

Figure 4.3: Probabilities $P_{\alpha\to\nu}$ $(\alpha = e, \mu, \tau)$ are binned in $\cos\theta, E$ space. The sharp change in features at $\cos\theta \approx -0.8$ is due to the higher density of the earth's core compared to the mantle.

Based on similar probability maps for different values of NSI parameters, one may simulate event counts binned in $\cos\theta, E, PID$ using Monte Carlo event generators. This analysis uses the FLERCNN reconstruction algorithm to generate counts for different parameter values, which is trained using the most-recently available DeepCore dataset

containing 150000 events over 9.28 years of operation. For the case of Standard Oscillations, the event counts are plotted in Fig.4.4.

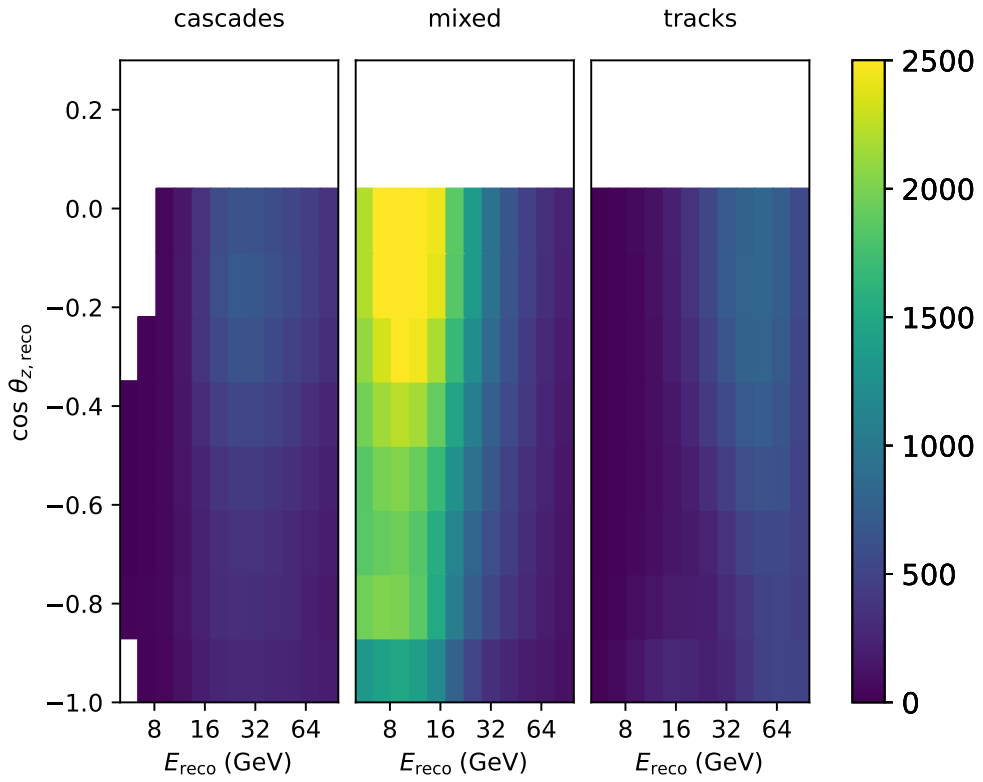

Figure 4.4: Event counts for the Standard Oscillations case. Certain bins are not considered in the analysis because of low event counts/bad modelling of ice properties [2].

4.1 NSI effects in IceCube

Due to stronger matter effects for smaller values of $\cos\theta$, NSI effects are more pronounced in those bins. In Fig.4.5, the counts for the standard oscillations case and for the corresponding case with the inverted mass ordering, along with the binned difference of counts is plotted.

As seen in Fig.4.5, the impact of NSI on observed counts is quite small, at least for the

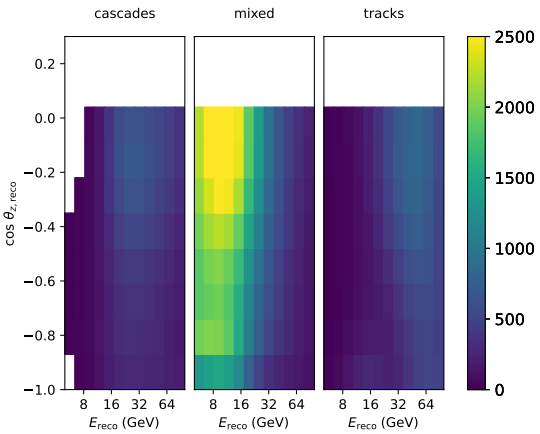

(a) $\varepsilon = 1, \phi_{12} = \phi_{13} = 0$ (NO)

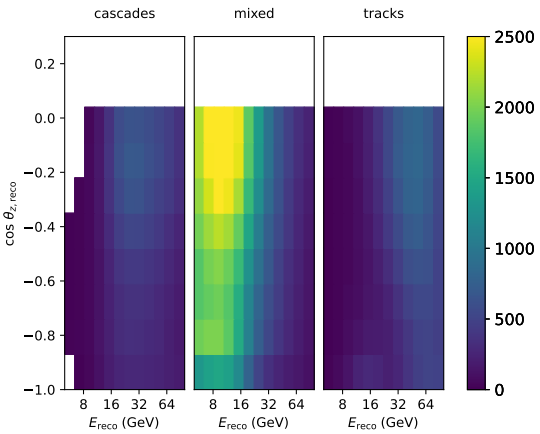

(b) $\varepsilon = -1, \phi_{12} = \phi_{13} = 0$ (IO)

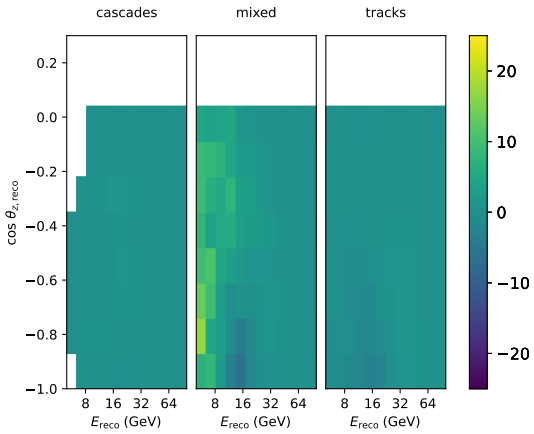

(c) Difference of counts (NO - IO)

Figure 4.5: The binned counts for a) $\varepsilon = 1, \phi_{12} = \phi_{13} = 0$ and b) $\varepsilon = -1, \phi_{12} = \phi_{13} = 0$ are plotted. The difference of counts is shown in c).

values shown. Examining the individual probabilities however paints a clearer picture, see Fig.(4.6).

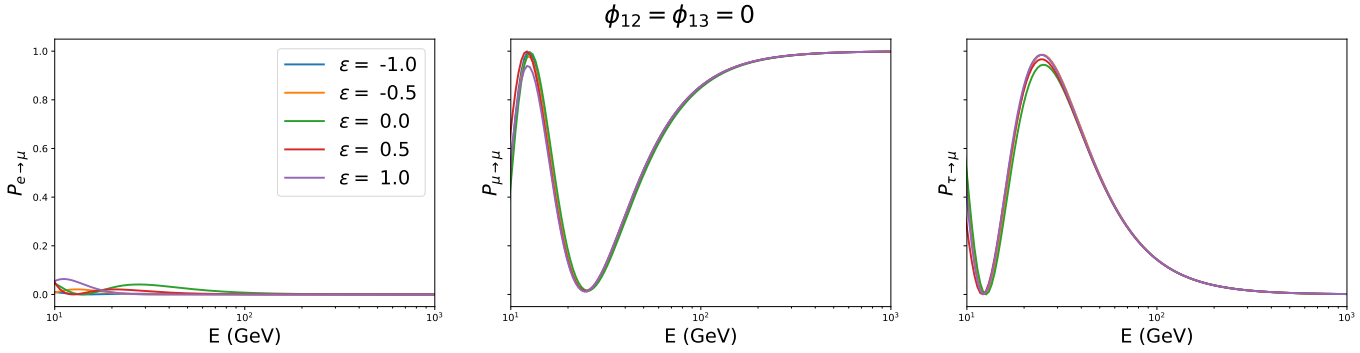

(a) ε

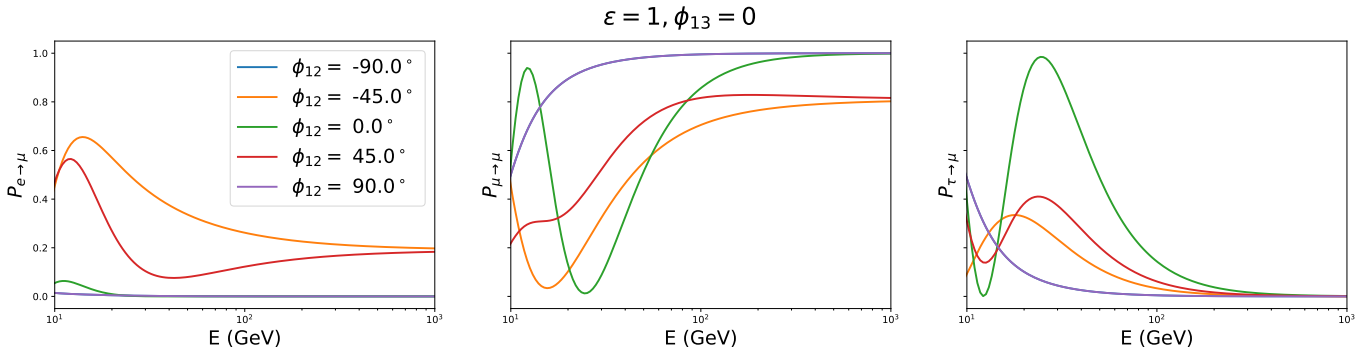

(b) ϕ_{12}

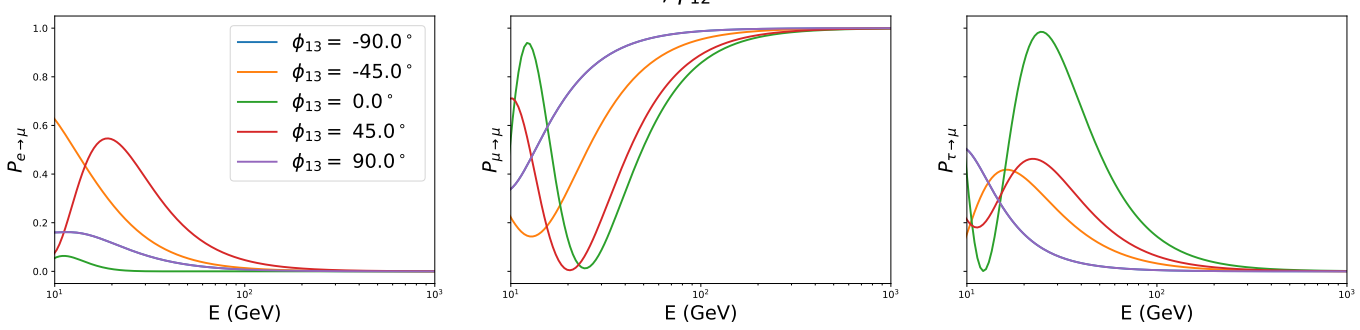

(c) ϕ_{13}

Figure 4.6: Impact of individual NSI parameters on oscillation probabilities.

Chapter 5

Constraining NSI

5.1 Analysis logistics

The nominal values and ranges of the PMNS matrix parameters are taken from the NuFit 4.0 results [8], and are provided in Table 5.1.

The nuisance parameters considered in the analysis can be classified as neutrino-cross section related parameters, scalar normalizations, or detector/ice systematics. The nominal values and ranges of these parameters are given in Table 5.2, 5.3, and 5.4 respectively.

As noted earlier, the parameter space considered in this analysis in much more complex than the analysis in [2], which included only one NSI parameter at a time. We wish to simultaneously constrain all NSI parameters, and the analysis is correspondingly expected to be significantly more computationally expensive.

To constrain any oscillation parameters using IceCube data, one must account for statistical fluctuations in any pseudo-data generated. For the observables of the analysis, statistical fluctuations cause for a $\Delta\chi^2 \approx 1$ with respect to the exact pseudo-data. To

Table 5.1: Taken from [2]. "Nominal values and allowed ranges of PMNS-matrix parameters in both mass orderings, as used for this analysis. Oscillation parameter values are based on the NuFIT 4.0 results [130, 131] including Super-K atmospheric data."

Parameter	Nominal value ± prior	Boundaries	Status
Y_e^I	0.4656	-	Fixed
Y_e^O	0.4656	-	Fixed
Y_e^M	0.4957	-	Fixed
Detector depth [km]	2.0	-	Fixed
Production height [km]	20.0	-	Fixed
θ_{23} [°]	45.3637	$[20, 70]$	Free
θ_{12} [°]	33.82	-	Fixed
δ_{CP} [°]	0	-	Fixed
Δm_{21} [eV^2]	0.0000739	-	Fixed
NO :			
θ_{13} [°]	8.61 ± 0.13	-	Fixed
Δm_{31} [eV^2]	0.00247996	$[0.0015, 0.003]$	Free
IO^2			
$\sin^2(\theta_{13})$ [°]	8.65 ± 0.13	-	Fixed
Δm_{31} [eV^2]	-0.00247996	$[-0.003, -0.0015]$	Free

Table 5.2: Taken from [2]. "Nuisance parameters considered with respect to neutrino cross sections, along with their priors and allowed ranges as well as their status during minimization. "

Parameter	Nominal Value	Boundaries	Status
M_A^{CCQE} (in σ)	0.0 ± 1.0	$\pm 2\sigma$	Free
M_A^{CCRES} (in σ)	0.0 ± 1.0	$\pm 2\sigma$	Free
DIS CSMS	0.0 ± 1.0	$\pm 3\sigma$	Free

Table 5.3: Taken from [2]. "Nuisance parameters that are constant scaling factors, along with their priors and allowed ranges as well as their status during minimization."

Parameter	Nominal Value	Boundaries	Status
N_ν	1	$[0.5, 2]$	Free
N_μ	1 ± 0.4	$[-2.25\sigma, +5\sigma]$	Free
N_{ν_τ}	1	$[0.0, 3.0]$	Fixed
$N_{\nu,NC}$	1 ± 0.2	$[0.5, 1.5]$	Fixed

Table 5.4: Taken from [2]. "Detector and ice related nuisance parameter values, along with their priors and allowed ranges where applicable."

Parameter	Nominal Value	Boundaries	Status
ϵ_{DOM}	1.0 ± 0.1	$[0.8, 1.2]$	Free
hole ice $p0$	0.101569	$[-0.6, 0.5]$	Free
hole ice $p1$	-0.049344	$[-0.15, 0.04]$	Free
bulk ice absorption	1.0 ± 0.05	$[0.9, 1.1]$	Free
bulk ice scattering	1.05 ± 0.1	$[0.85, 1.25]$	Free
N_{bfr}	0.0	$[0.0, 1.0]$	Free

tackle this, IceCube analyses are structures in an optimal manner. First, one must obtain a minimization strategy that can recover pseudo-data from an injected hypothesis reasonably well, while neglecting statistical fluctuations (the so-called Asimov case). Once this is achieved, one averages over ~ 20 simulated datasets for every hypothesis during the minimization procedure, while allowing for statistical fluctuations. In this work, we obtain an optimal minimization procedure for the asimov case, along with the corresponding sensitivities of IceCube to NSI. This sets up the remaining analysis to obtain competitive constraints on NSI.

5.2 Selecting nuisance parameters

Since the complexity of the minimization process will increase with the dimensionality of the parameter space, it is essential eliminate find any nuisance parameters which have a very minor impact on the the NSI constraints. This is done using the so-called $N-1$ tests [2], done for each NSI parameter: a hypothesis with the nuisance parameter of interest n having a true value away from the nominal value (taken to be 1σ away, or half the difference between the nominal value and the upper limit of n). With this, 2 fits are done: the null fit, where the NSI parameter is fixed to the truth value, and the free fit, where the NSI parameter is free. Then, the difference between the metric values of

these fits m is used to quantify the impact of n on recovering NSI hypotheses:

$$m = \Delta\chi^2_{mod} = \chi^2_{\text{null}} - \chi^2_{\text{free}} \tag{5.1}$$

In [2], this was performed for individual NSI parameters in the standard NSI parameterization (Eq.(2.27)), and nuisance parameters with $m > 0.1\sigma$ were kept free. The individual impact of each nuisance parameter on the analysis in [2] is shown in Fig.5.1. As a starting point for this analysis, we use the same nuisance parameters as the ones used in [2]. This test shall be repeated for the Generalized Matter Potential at a later time.

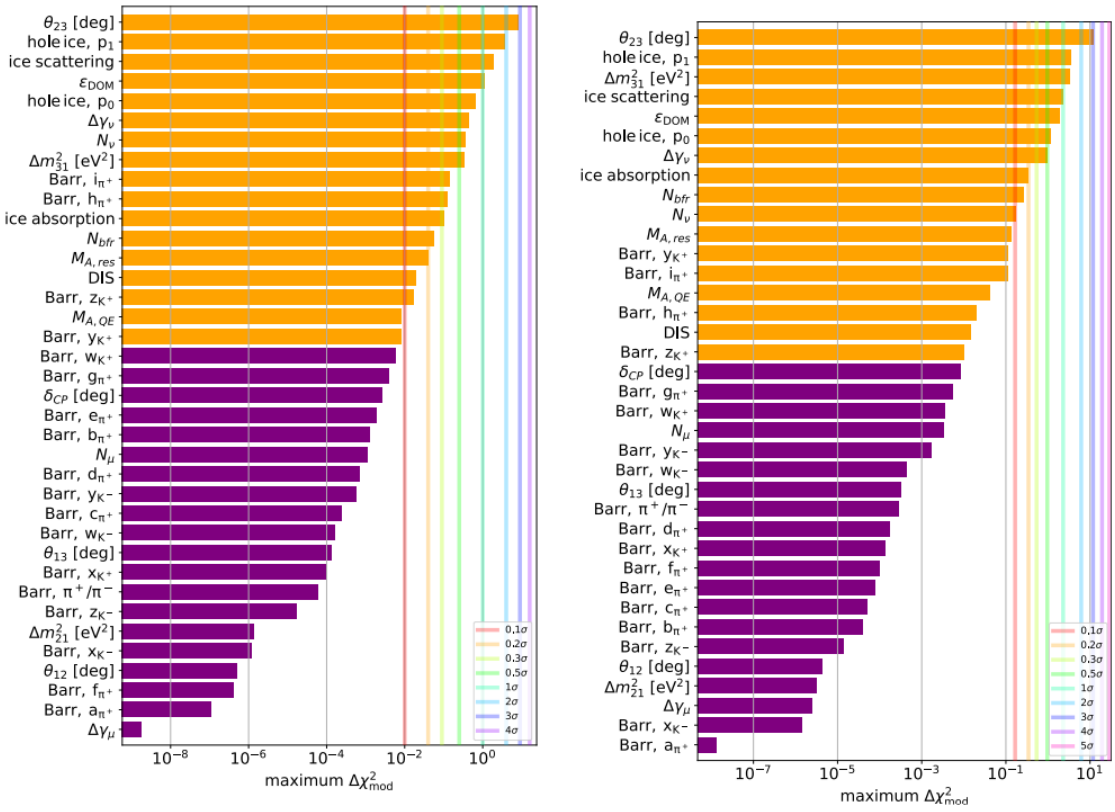

Figure 5.1: Taken from [2] "Impact of fixing individual nuisance-parameters to their nominal value when fitting to an off-nominal hypothesis. The figures for $\varepsilon^{\oplus}_{e\mu}$ and $\varepsilon^{\oplus}_{\mu\tau}$ can be found in appendix section B.6."

5.3 Recovering NSI hypotheses

Let us consider constructing pseudo-data for a particular NSI hypothesis. An optimal minimization procedure should be able to recover the injected hypothesis with a reasonable success rate.

The minimization procedure considered in [2] provides a good starting point to obtain a procedure for our higher-dimensional parameter space. It has been observed that there are various symmetries in the parameter space of the Generalized Matter Potential. The exact symmetries have been discussed in [6], however there are also 'non-exact' symmetries, in which certain points in the NSI space mimic (not exactly) points obtained by inverting the signs of one of the NSI parameters, or flipping θ_{23} about $\frac{\pi}{4}$. When minimizing with respect to a particular NSI hypothesis, this translates to the various 'reflected' hypothesis being local minima in the parameter space. Thus, we perform a minimization in each of the $2^4 = 16$ possible orthants, where each orthant is obtained by choosing a positive or negative sign for each NSI parameter, and $\theta_{23} > \frac{\pi}{4} or \theta_{23} < \frac{\pi}{4}$.

As discussed in [2], the parameter space with even a single NSI parameter is quite complicated. One finds that simply using one instance of common minimization algorithms that start from a fixed point typically converge to local minima, while algorithms which do not require a fixed starting point require extremely large computational resources. Thus, one uses a global minimization algorithm to tune the starting point of a subsequent faster minimization algorithm.

The structure of our minimization approach is similar to the one used in [2]. First, an instance of the Controlled Randomized Search 2 (CRS2) [9] is called in each of the 16 orthants. Each instance creates a random population of points in the respective orthant. This population is used to slowly tune a point that, given enough population size, slowly converges to the global minimum. The algorithm details can be found in [9].

After a certain threshold on the run time/the number of function evaluations, or on the difference in the function value between two consecutive iterations of the algorithm, is reached , one obtains a 'tuned' point in the parameter space. The tuned point in each orthant is compared to the injected hypothesis, and the point that provides the least metric value is reflected in to all the other orthants. Then, an instance of the SUBPLEX algorithm [10] is called in each orthant, starting at the reflected best point from the CRS2 algorithm. The result of the SUBPLEX algorithm in each orthant is further polished by a single instance of the iminuit algorithm [11], a local-gradient based minimization algorithm. Finally, the best result among all orthants is chosen. All instances of each algorithm are run in parallel, requiring 16 CPUs per minimization.

If the result of the CRS2 algorithm is reasonably close to the global optimum, ther SUBPLEX algorithm takes minimal computational resources (30-90 minutes per instance). In [2], a population of 250 points, with a threshold run time of 2 hours was found to be sufficient for the tuned point to be reasonably close to the global optimum. This was found to be inadequate for our parameter space. To reach the required population and run-times for the CRS2 algorithm, a step-wise approach to include nuisance parameters was taken. As shown in [9], the typically recommended emperical population N for an n-dimensional optimization problem grows linearly with n

$$N = 10(n + 1) \tag{5.2}$$

Starting with considering only NSI parameters in the minimization, the minimization settings were adjusted till injected hypothesis were recovered reasonably well. Nuisance parameters were then added in order of their effects on NSI fits as documented in [2] (see Fig.5.1). Once all the nuisance parameters were included (at a $\Delta\chi^2 = 0.1\sigma$ in

Fig.5.1), a population of 900 points, with a maximum run-time of 72 hours was found to return points close to the injected hypotheses with a reasonable success rate. The results of this minimization algorithm in recovering various injected hypotheses are shown in Figs.5.2, 5.3, and 5.4, where points from a 4*4*4 grid of points in the $\varepsilon - \phi_{12} - \phi_{13}$ space were injected and recovery was attempted; around 67% of the points were recovered successfully. All put together, each minimization takes up to 72.16 = 1152 CPU hours.

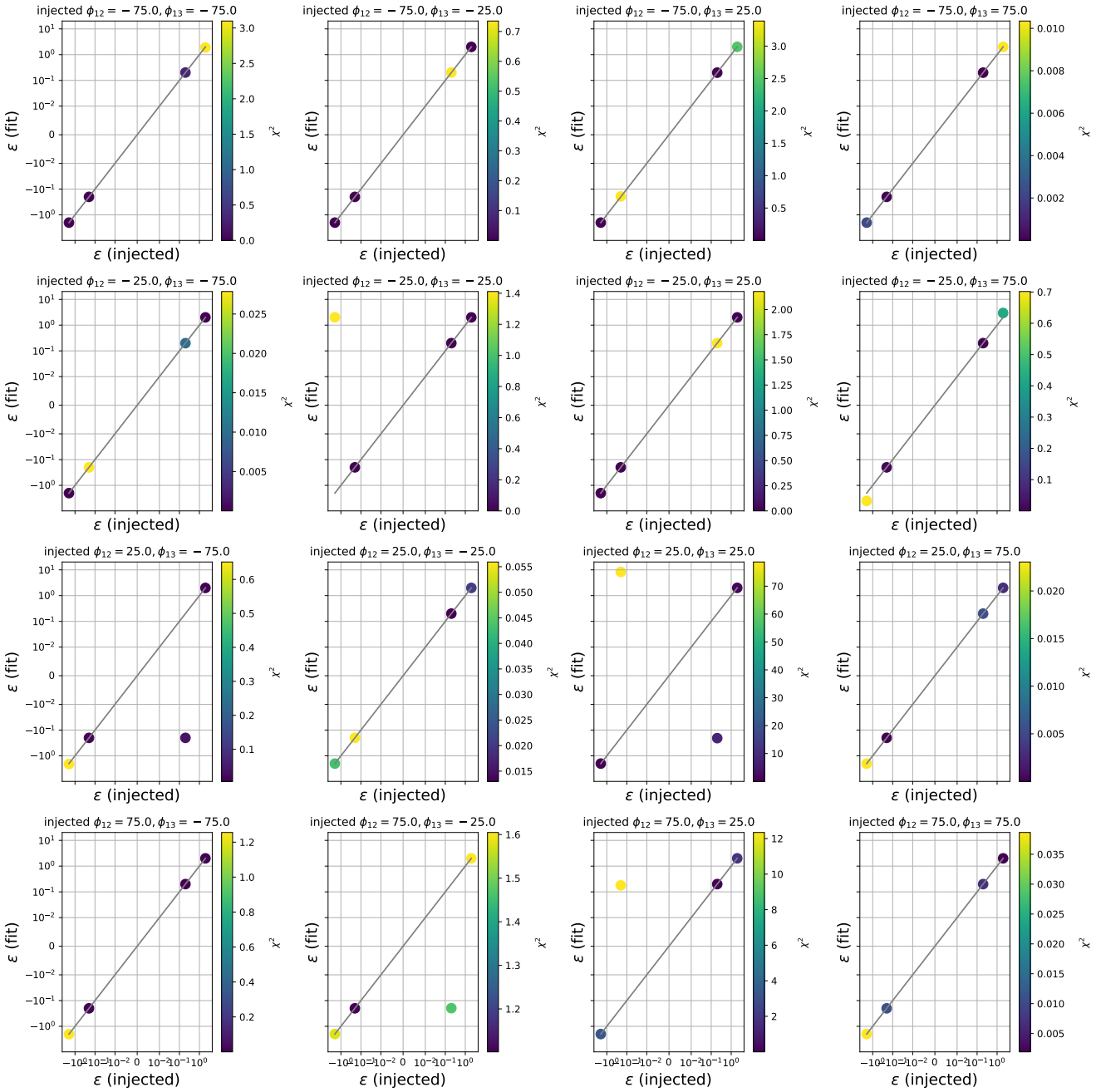

Figure 5.2: Recovery of ε in various NSI hypotheses using the minimization process in Section 5.3 is shown. The true values of ε for each hypotheses is represented on the x axis, while the recovered value is on the y axis. The ideal recovery case $y = x$ is marked by a grey line. The χ^2 value of each fit is indicated using a color bar. The true values of ϕ_{12}, ϕ_{13} in each hypothesis is noted in the title of each plot. For all points, minimization is done over all NSI parameters and all nuisance parameters.

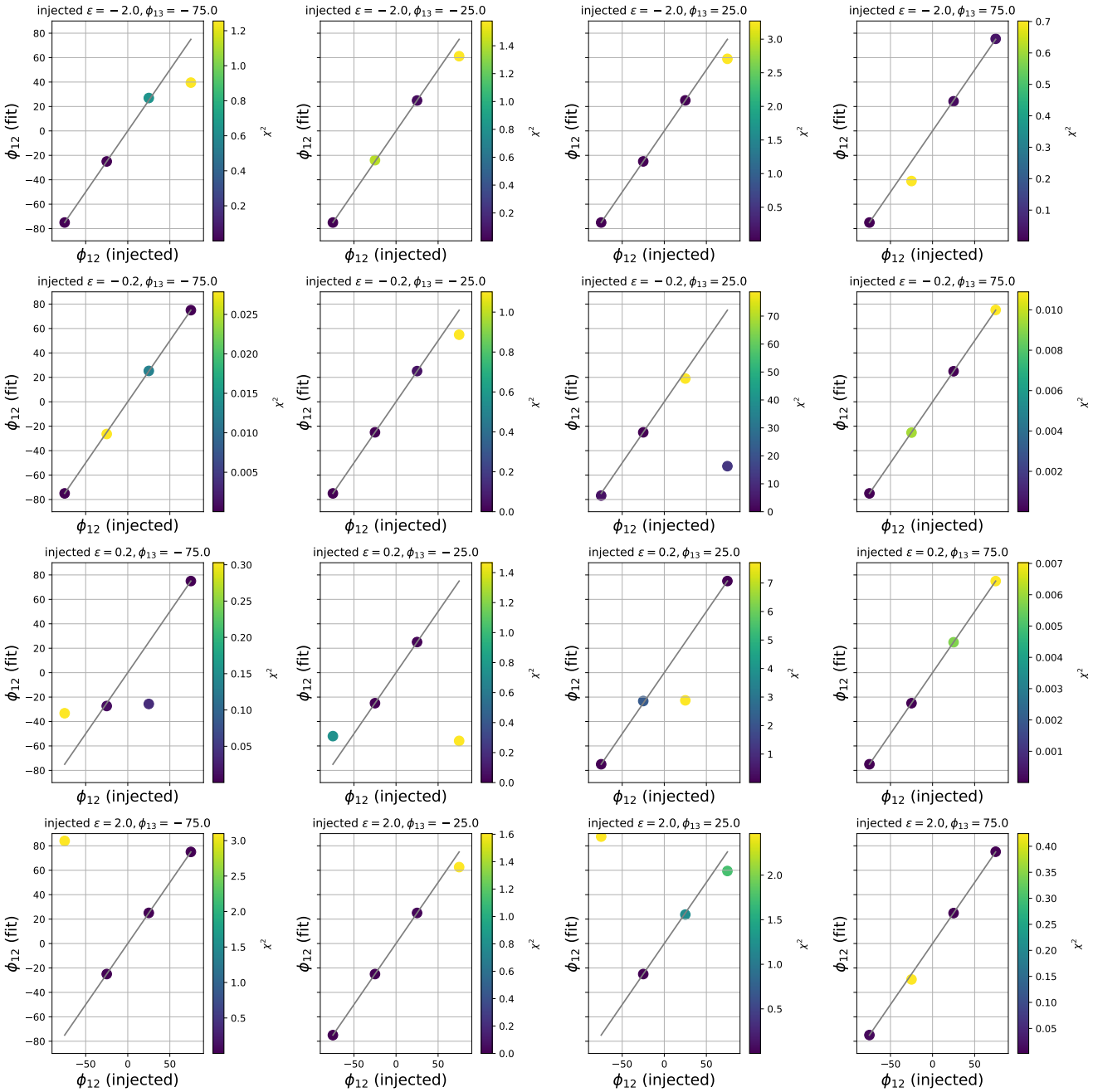

Figure 5.3: Recovery of ϕ_{12} in various NSI hypotheses using the minimization process in Section 5.3.

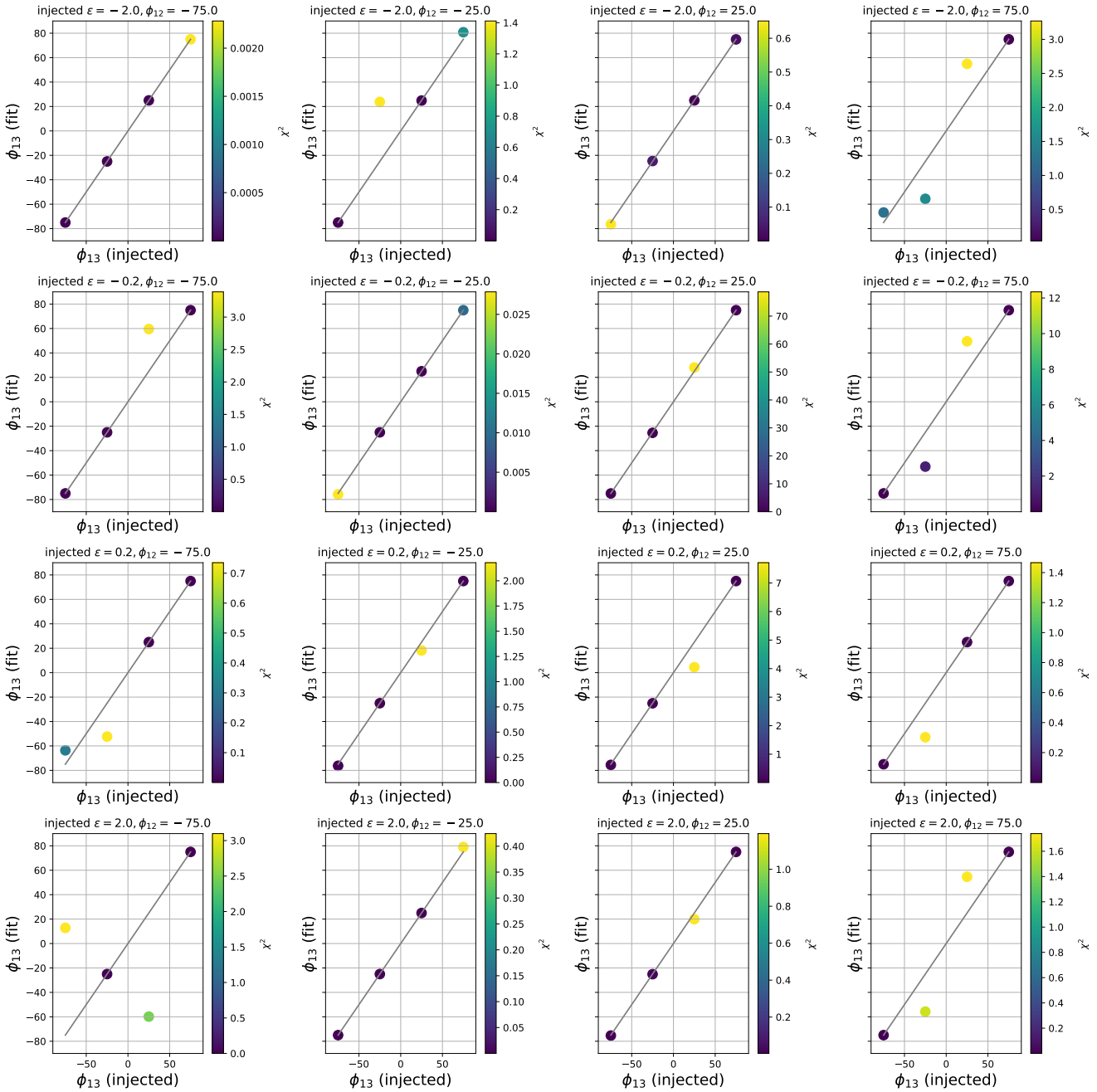

Figure 5.4: Recovery of ϕ_{13} in various NSI hypotheses using the minimization process in Section 5.3.

5.4 NSI sensitivities

Having found an optimized minimization procedure, we can now produce expected sensitivities of IceCube to the NSI parameters. In other words, we wish to estimate how well IceCube can distinguish between the case of Standard Oscillations, with all nuisance parameters at their nominal values, and another NSI hypothesis with nuisance parameters anywhere in their respective ranges. This is the first step towards any further analysis to place NSI constraints.

The sensitivities of individual NSI parameters are given in Fig.5.5. To construct sensitivities with respect to a particular NSI parameter, one fixes the parameter to some value away from its no-NSI value, and minimizes the χ^2 metric over all the remaining parameters. One repeats this for various hypothetical values of the parameter of interest.

To better visualize the NSI parameter space, one may consider the 2-parameter sensitivities in the NSI space, where 2 NSI parameters are simultaneously shifted away from their no-NSI values, and the metric is minimized over all the remaining parameters. These sensitivities are shown in Fig.5.6. Accounting for the high computational costs, a rather poor resolution of 21 points in ε and 15 points in ϕ_{12} and ϕ_{13} each is chosen. The one-dimensional projections along both axis are also provided, which should match the corresponding single-parameter sensitivities (the low resolution in the 2-dimensional sensitivities can create some deviations). This is verified to be the case.

As mentioned earlier, this analysis uses a livetime of 9.28 years, as opposed to 2.5 years in [1]. Thus, we can compare our sensitivities with those obtained in [1]; as one would expect, we see an overall increase in sensitivities due to the higher livetime and better reconstruction algorithms. In particular, we can place 1σ CL limits on the sensitivities of each NSI parameter; no such limits could be placed in [1]. These limits are stated in Table 5.5.

Table 5.5: 1σ CL sensitivities for each NSI parameter obtained from Fig.5.5

Parameter	1σ CL	No-NSI value
ε	$(-1.77, -0.38) \cup (0.36, 2.61)$	1
ϕ_{12}	$(-4.25°, 4.5°)$	0
ϕ_{13}	$(-8.78°, 9.88°)$	0

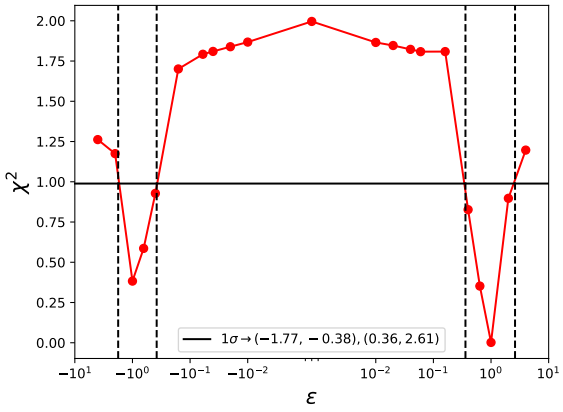

(a) ε

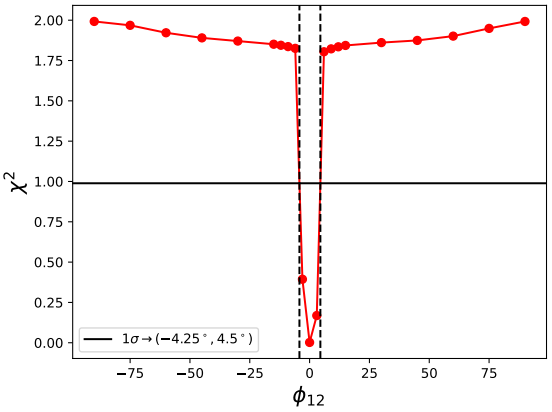

(b) ϕ_{12}

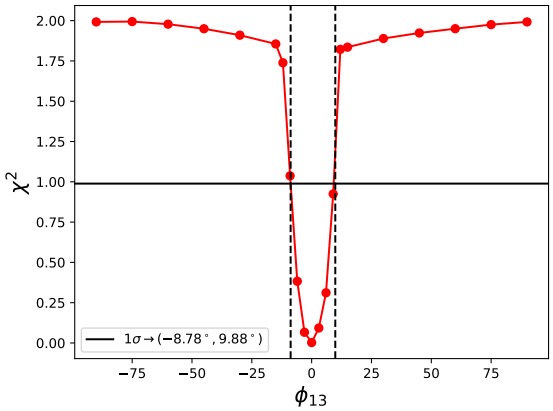

(c) ϕ_{13}

Figure 5.5: Sensitivities to the no-NSI hypothesis ($\varepsilon = 1, \phi_{12} = \phi_{13} = 0$)for each individual NSI parameter are shown. For each plot, minimization is done over all nuisance parameters and the NSI parameters not being varied in the plot. The 1σ CL limits are indicated in each plot.

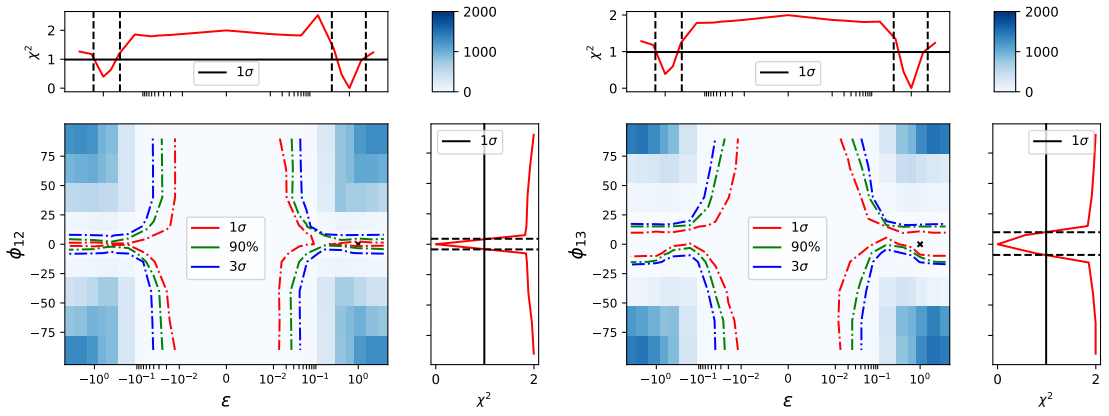

(a) $\varepsilon - \phi_{12}$ (b) $\varepsilon - \phi_{13}$

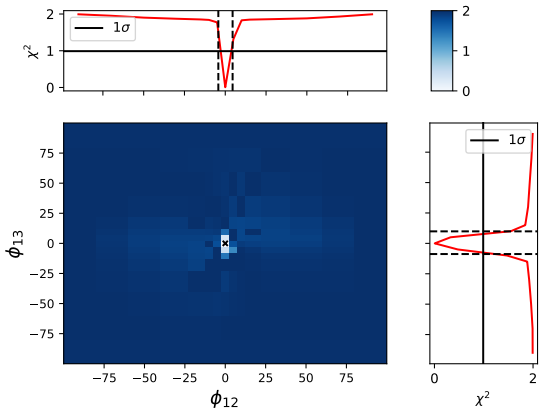

(c) $\phi_{12} - \phi_{13}$

Figure 5.6: To better visualize the NSI parameter space, sensitivities to the no-NSI hypothesis (marked by x) for 2-NSI parameter spaces are shown. For each plot, minimization is done over all nuisance parameters and the NSI parameters not being varied in the plot. $1\sigma, 90\%$, and 3σ CL contours are indicated. The one dimensional projections, obtained by minimizing χ^2 along one of the axes, are shown as well. The 1σ CL limits obtained in Fig.5.5 are marked in the projections. They are seen to nearly match the limits one would obtain from the projection. Small differences in these limits can be attributed to the resolution of the 2 dimensional sensitivities.

Chapter 6

Conclusion

The asimov sensitivities of IceCube to the no-NSI hypothesis are presented. We first parameterize neutrino oscillations in vacuum, whereby the flavor neutrino states are assumed to be superposition of non-degenerate massive neutrino eigenstates, with the respective linear combinations given by the PMNS matrix U. Then, we incorporate matter effects in oscillations via a matter Hamiltonian created by CC and NC scattering of neutrinos with electrons, protons, and neutrons.

We parameterize neutrino NSI via effective coupling strengths $\varepsilon_{\alpha\beta}$ which act as a perturbation to the matter Hamiltonian. This results in 8 independent NSI parameters. To simplify the parameter space, we adopt a reparameterization of NSI effects called the Generalized Matter Potential, which assumes that two eigenvalues of the matter Hamiltonian are degenerate; under this regime, there is a strong cancellation of NSI effects, which would lead to the weakest possible constraints. We finally have 3 independent NSI parameters: $\varepsilon, \phi_{12}, \phi_{13}$.

The neutrino signatures in IceCube are briefly discussed, and the counts of neutrino events binned in these signatures, along with the neutrino energy and the incoming

direction of the neutrino, form the main observable of this analysis.

A procedure to reasonably (67% success rate) recover various NSI hypothesis by minimizing the χ^2 metric with respect to the true hypothesis in the NSI + nuisance parameter space is constructed (for the asimov case). Finally, using this procedure, the asimov NSI sensitivities are shown, with the 1σ CL limits presented in Table 5.5.

Bibliography

[1] IceCube collaboration. All-flavor constraints on nonstandard neutrino interactions and generalized matter potential with three years of icecube deepcore data. *Phys. Rev. D*, 104:072006, Oct 2021.

[2] E. Lohfink. Testing nonstandard neutrino interaction parameters with icecube-deepcore. *Ph.D. thesis, Johannes Gutenberg University of Mainz*, 2023.

[3] Y. Farzan and M. Tortola. Neutrino oscillations and non-standard interactions. *Frontiers in Physics*, 6, 2018.

[4] O G Miranda and H Nunokawa. Non standard neutrino interactions: current status and future prospects. *New J. Phys*, 17, 2015.

[5] P. S. Bhupal Dev, K. S. Babu, and Peter B. Denton et al. Neutrino non-standard interactions: A status report. *SciPost Phys. Proc.*, page 001, 2019.

[6] M. C. Gonzalez-Garcia, M. Maltoni, and J. Salvado. Testing matter effects in propagation of atmospheric and long-baseline neutrinos. *JHEP*, 05:075, 2011.

[7] A. Friedland, C. Lunardini, and M. Maltoni. Atmospheric neutrinos as probes of neutrino-matter interactions. *Phys. Rev. D*, 70:111301, Dec 2004.

[8] V. Esteban, M. C. Gonzalez-Garcia, A. Hernandez-Cabezudo, M. Maltoni, and T. Schwetz. Global analysis of three-flavour neutrino oscillations: synergies and

tensions in the determination of θ_{23}, δ_{CP}, and the mass ordering. *Journal of High Energy Physics*, 2019.

[9] W.L. Price. Global optimization by controlled random search. *J Optim Theory Appl*, 1983.

[10] W.L. Price. Functional stability analysis of numerical algorithms. *Ph.D. thesis, Department of Computer Sciences, University of Texas at Austin*, 1990.

[11] F. James and M. Roos. Minuit - a system for function minimization and analysis of the parameter errors and correlations. *Computer Physics Communications*, 10(6):343–367, 1975.